

## Supporting Information

### Phase Transition Engineering to Break the Symmetry of Diamond-Like Chalcogenide for Second-Order Nonlinear Optics

*Chunlan Tang,<sup>ab</sup> Aoge Yao,<sup>c</sup> Wenhao Xing,<sup>d</sup> Wenwen Jiang,<sup>b</sup> Jian Tang,<sup>b</sup> Lei Kang,<sup>c</sup> Jieyun Wu,<sup>\*a</sup> Wenlong Yin<sup>\*b</sup> and Bin Kang<sup>b</sup>*

<sup>a</sup> School of Optoelectronic Science and Engineering, University of Electronic Science and Technology of China, Chengdu 611731, P.R. China.

<sup>b</sup> Institute of Chemical Materials, China Academy of Engineering Physics, Mianyang 621900, P.R. China.

<sup>c</sup> Beijing Center for Crystal Research and Development, Key Laboratory of Functional Crystals and Laser Technology, Technical Institute of Physics and Chemistry, Chinese Academy of Sciences, Beijing 100190, P.R. China.

<sup>d</sup> School of Mechanical and Electrical Engineering, Henan Institute of Science and Technology, Xinxiang 453003, P. R. China.

E-mail: [jieyunwu@uestc.edu.cn](mailto:jieyunwu@uestc.edu.cn)

E-mail: [wlyin@caep.cn](mailto:wlyin@caep.cn)

## Table of Contents

Section	Title	Page
Section S1	Synthesis, characterization, and computational methods.	S3-5
Table S1	Crystallographic data and structure refinement.	S6
Table S2	Atomic coordinates, equivalent isotropic displacement parameters, and bond valence sums (BVS) for $\alpha$ -Ag <sub>4</sub> P <sub>2</sub> S <sub>7</sub> .	S7
Table S3	Selected band distances (Å) and band angles (°) for $\alpha$ -Ag <sub>4</sub> P <sub>2</sub> S <sub>7</sub> .	S8
Table S4	Atomic coordinates, equivalent isotropic displacement parameters, and bond valence sums (BVS) for $\beta$ -Ag <sub>4</sub> P <sub>2</sub> S <sub>7</sub> .	S9
Table S5	Selected band distances (Å) and band angles (°) for $\beta$ -Ag <sub>4</sub> P <sub>2</sub> S <sub>7</sub> .	S10
Table S6	Band gap comparison in ternary Ag-based DL chalcogenides.	S11
Fig. S1	The coordination environments of Ag1, Ag2, and P atoms of $\alpha$ -Ag <sub>4</sub> P <sub>2</sub> S <sub>7</sub> (a, b, and c) and $\beta$ -Ag <sub>4</sub> P <sub>2</sub> S <sub>7</sub> (d, e, and f).	S12
Fig. S2	Peritectic reaction of Ag <sub>7</sub> P <sub>3</sub> S <sub>11</sub> and melt.	S12
Fig. S3	UV-vis-NIR diffuse reflectance spectra of $\alpha$ -Ag <sub>4</sub> P <sub>2</sub> S <sub>7</sub> .	S13
Fig. S4	The SEM pictures and EDS results of $\beta$ -Ag <sub>4</sub> P <sub>2</sub> S <sub>7</sub> .	S13
Fig. S5	The coordination environments of [Ag <sub>1</sub> S <sub>4</sub> ] <sup>7-</sup> bridges in (a) $\alpha$ -Ag <sub>4</sub> P <sub>2</sub> S <sub>7</sub> and (b) $\beta$ -Ag <sub>4</sub> P <sub>2</sub> S <sub>7</sub> .	S14
Fig. S6	SHG signals to compare between $\beta$ -Ag <sub>4</sub> P <sub>2</sub> S <sub>7</sub> and references at the particle size of 150–200 $\mu$ m.	S14
Fig. S7	UV-vs-NIR diffuse reflectance spectra of $\beta$ -Ag <sub>4</sub> P <sub>2</sub> S <sub>7</sub> .	S15
Fig. S8	Raman spectrum of $\beta$ -Ag <sub>4</sub> P <sub>2</sub> S <sub>7</sub> .	S15
References		S16

## 1. Section S1

### Synthesis of $\alpha$ -Ag<sub>4</sub>P<sub>2</sub>S<sub>7</sub> and $\beta$ -Ag<sub>4</sub>P<sub>2</sub>S<sub>7</sub>.

All the raw materials, including Ag<sub>2</sub>S (99.999%, Aladdin) and P<sub>2</sub>S<sub>5</sub> (99%, Aladdin), were stored in a glovebox filled with argon (keeping moisture and oxygen lower than 0.1 ppm). A glovebox or vacuum was used to complete all preparation processes.

The single crystals and the polycrystalline sample of  $\alpha$ -Ag<sub>4</sub>P<sub>2</sub>S<sub>7</sub> were initially prepared by traditional high-temperature solid-state reaction of Ag<sub>2</sub>S (10 mmol) and P<sub>2</sub>S<sub>5</sub> (5 mmol). The mixture was thoroughly ground in an agate mortar and loaded into silica tubes. The silica tubes were sealed with oxy-hydrogen flame under 10<sup>-3</sup> Pa and then placed in a computer-controlled furnace. The following temperature control program was executed: heating from room temperature to 673 K in 10 h, kept for 72 h, and cooled to room temperature. Yellowish transparent block crystals and the polycrystalline sample  $\alpha$ -Ag<sub>4</sub>P<sub>2</sub>S<sub>7</sub> were obtained. The samples were pure enough confirmed by the powder X-ray diffraction (PXRD) measurement.

The single crystals of  $\beta$ -Ag<sub>4</sub>P<sub>2</sub>S<sub>7</sub> were initially prepared by traditional high-temperature solid-state reaction of Ag<sub>2</sub>S (992 mg) and P<sub>2</sub>S<sub>5</sub> (444 mg). The mixture was thoroughly ground in an agate mortar and loaded into silica tubes. The silica tubes were sealed with oxy-hydrogen flame under 10<sup>-3</sup> Pa and then placed in a computer-controlled furnace. The following temperature control program was executed: heating from room temperature to 673 K in 10 h, kept for 3 h, and cooled to room temperature. Yellowish transparent block crystals were obtained. The elemental composition analysis of the single crystal was tested on the Energy-dispersive X-ray (EDX) equipment, carried out on a Hitachi S-4800 scanning electron microscope. It showed that Ag, P and S elements were homogeneously distributed in the crystals with an approximate molar ratio of 4: 2: 7 (Fig. S1). The polycrystalline sample Ag<sub>4</sub>P<sub>2</sub>S<sub>7</sub> was obtained by reacting Ag<sub>2</sub>S (10 mmol) and P<sub>2</sub>S<sub>5</sub> (5 mmol) in sealed evacuated fused-silica tubes. The tubes were heated to 903 K in 10 h in a computer-controlled furnace, kept for 120 h, and then cooled to room temperature. The samples were pure enough confirmed by the powder X-ray diffraction (PXRD) measurement.

### X-ray Diffraction Analysis.

Single-crystal X-ray diffraction (SCXRD) data were collected on a Rigaku XtaLAB Synergy

four-circle diffractometer with Mo-K $\alpha$  radiation ( $\lambda = 0.71073 \text{ \AA}$ ). The structure was solved with the ShelXT structure solution program using Intrinsic Phasing and refined with the ShelXL refinement package using Least Squares minimisation. The detailed crystallographic data and refinement parameters of the compounds are listed in Table S1. The atomic coordinates, equivalent displacement parameters, calculated bond valence sums (BVSs) and the important bond lengths and angles are shown in Tables S2-S5S1-S4.

### **Powder X-ray Diffraction.**

The powder X-ray diffraction pattern of the as-obtained polycrystalline powders were performed at room temperature on a Bruker D8 Focus diffractometer with Cu K $\alpha$  ( $\lambda = 1.5418 \text{ \AA}$ ) radiation. The scanning step width of  $0.03^\circ$  and a fixed counting time 0.2 s/step were applied to record the patterns in the  $2\theta$  range of  $10\text{--}70^\circ$ . The experimental PXRD pattern of the Ag<sub>4</sub>P<sub>2</sub>S<sub>7</sub> matches well with the ones simulated from the single-crystal structure determination, indicated high purity of the polycrystalline sample.

### **Diffuse reflectance spectroscopy.**

The diffuse reflectance spectrum was carried out on a Cary 7000 UV-vis-NIR spectrophotometer equipped with a diffuse reflectance accessory in the wavelength range of 250 nm to 2500 nm. And the polytetrafluoroethylene (PTFE) was used as a 100% reflectance standard. The absorption spectrum was calculated from the reflection spectrum by the Kubelka-Munk function.<sup>1</sup>

### **Raman Spectra.**

The Raman spectra were recorded on a Lab RAM Aramis spectrometer equipped with a 532 nm laser at room temperature on polycrystalline powder with a spectral resolution of  $1 \text{ cm}^{-1}$ .

### **Thermal Analysis.**

The differential scanning calorimeter (DSC) analysis was performed on the Labsys EVO TG/DTA/DSC 1600 °C (SETARAM) thermal analyzer. Polycrystalline samples  $\alpha$ -Ag<sub>4</sub>P<sub>2</sub>S<sub>7</sub> were sealed within small fused-silica tubes, which were evacuated to  $10^{-3} \text{ Pa}$  and heated from room temperature to 1073 K at the rate of 10 K/min. Polycrystalline samples  $\beta$ -Ag<sub>4</sub>P<sub>2</sub>S<sub>7</sub> were sealed within small fused-silica tubes, which were evacuated to  $10^{-3} \text{ Pa}$  and heated from room

temperature to 973 K at the rate of 10 K/min.

### **Measurements of Second-Harmonic Generation (SHG).**

The SHG responses were tested by the Kurtz-Perry method employing a Q-switched laser (2100 nm, 1 Hz, 50 ns) as fundamental light.<sup>2</sup> The polycrystalline powder of  $\beta$ -Ag<sub>4</sub>P<sub>2</sub>S<sub>7</sub> was thoroughly ground and sieved into several desired particle size ranges of 20–40, 40–74, 74–105, 105–150 and 150–200  $\mu$ m. These samples were then put into a customized sample cell with a sample thickness of 1 mm. Commercial microcrystalline AgGaS<sub>2</sub> samples of the same particle size range were selected as the references.

### **Computational methods.**

The first-principles calculation of  $\beta$ -Ag<sub>4</sub>P<sub>2</sub>S<sub>7</sub> was performed by CASTEP program based on plane-wave pseudopotential density functional theory (DFT).<sup>3, 4</sup> The exchange-correlation energy was described by Perdew-Burke-Ernzerhof (PBE) functional within the framework of generalized gradient approximation (GGA).<sup>5, 6</sup> The optimized norm-conserving pseudopotentials in the Kleinman-Bylander form, which allows the employment of a relatively small plane-wave basis set without compromising the computational accuracy, were used to describe the interaction between the atomic cores and valence electrons. Ag  $4d^{10}5s^1$ , P  $3s^23p^3$  and S  $3s^23p^4$  were treated as valence electrons.<sup>7</sup> The kinetic energy cut off of 500 eV with Monkhorst-Pack k-point meshes spanning less than  $0.04/\text{\AA}^3$  were chosen in the Brillouin zone. The optical properties were calculated using the scissors-corrected PBE method,<sup>8</sup> where the scissors operator was set to the difference between the experimental and PBE band gaps. Based on the electronic band structure, the imaginary part of the dielectric function was calculated and the real part of the dielectric function was determined by means of the Kramers-Kronig transform, from which the refractive indices and the birefringence  $\Delta n$  were deduced. The SHG-weighted charge density analysis tools are employed to analyze the contribution of the respective parts to the nonlinear optical (NLO) properties.<sup>9</sup> Based on the technical analysis, the origins of the SHG effects can be illustrated in a clear way.

## 2. Tables and Figures

**Table S1.** Crystallographic data and structure refinement.

Formula	$\alpha$ -Ag <sub>4</sub> P <sub>2</sub> S <sub>7</sub>	$\beta$ -Ag <sub>4</sub> P <sub>2</sub> S <sub>7</sub>
Formula weight	717.84	717.84
Temperature/K	295.52(10)	295.8(4)
Crystal system	monoclinic	trigonal
Space group	<i>C2/c</i>	<i>P3<sub>2</sub>21</i>
<i>a</i> = /Å	10.7634(8)	6.3563(5)
<i>b</i> = /Å	6.5280(4)	6.3563(5)
<i>c</i> = /Å	16.1759(13)	23.3477(18)
$\alpha$ = /°	90	90
$\beta$ = /°	106.734(8)	90
$\gamma$ = /°	90	120
Volume/Å <sup>3</sup>	1088.44(14)	816.93(14)
Z	4	3
$\rho$ /(g/cm <sup>3</sup> )	4.381	4.377
$\mu$ /mm <sup>-1</sup>	8.667	8.661
F(000)	1320.0	990.0
Radiation	Mo K $\alpha$ ( $\lambda$ = 0.71073)	Mo K $\alpha$ ( $\lambda$ = 0.71073)
2 $\theta$ range for data collection (°)	5.26 to 52.736	5.234 to 52.678
Index ranges	-13 ≤ <i>h</i> ≤ 12, -8 ≤ <i>k</i> ≤ 8, -19 ≤ <i>l</i> ≤ 20	-7 ≤ <i>h</i> ≤ 4, -7 ≤ <i>k</i> ≤ 7, -27 ≤ <i>l</i> ≤ 29
Reflections collected	4585	33563
Independent reflections	1109 [ <i>R</i> <sub>int</sub> = 0.0567, <i>R</i> <sub>sigma</sub> = 0.0410]	1097 [ <i>R</i> <sub>int</sub> = 0.0490, <i>R</i> <sub>sigma</sub> = 0.0454]
data/restraints/parameters	1109/0/62	1097/0/60
GOOF on F <sup>2</sup>	0.988	0.929
<i>R</i> <sub>1</sub> , <i>wR</i> <sub>2</sub> ( <i>I</i> > 2 $\sigma$ ( <i>I</i> ))	<i>R</i> <sub>1</sub> = 0.0465, <i>wR</i> <sub>2</sub> = 0.1472	<i>R</i> <sub>1</sub> = 0.0395, <i>wR</i> <sub>2</sub> = 0.1187
<i>R</i> <sub>1</sub> , <i>wR</i> <sub>2</sub> [all data]	<i>R</i> <sub>1</sub> = 0.0540, <i>wR</i> <sub>2</sub> = 0.1655	<i>R</i> <sub>1</sub> = 0.0426, <i>wR</i> <sub>2</sub> = 0.1223
Largest diff. peak/hole (e Å <sup>-3</sup> )	0.38/-0.66	2.18/-1.77
Flack parameter	/	-0.14(6)

$$R_1 = \frac{\sum ||F_o| - |F_c||}{\sum |F_o|}, \quad wR_2 = \left[ \frac{\sum w(F_o^2 - F_c^2)^2}{\sum w(F_o^2)^2} \right]^{1/2}$$

**Table S2.** Atomic coordinates, equivalent isotropic displacement parameters and bond valence sums (BVS) for  $\alpha$ -Ag<sub>4</sub>P<sub>2</sub>S<sub>7</sub>.

Atom	Wyckoff position	x	y	z	U <sub>eq</sub> (Å <sup>2</sup> ) <sup>a</sup>	BVS
Ag1	8f	0.96071(10)	0.28118(17)	0.44750(7)	0.0575(13)	1.03
Ag2	8f	0.75493(11)	0.69965(14)	0.34138(7)	0.0572(13)	1.06
P1	8f	0.6084(2)	0.1756(4)	0.35543(16)	0.0342(14)	5.19
S1	8f	0.6744(2)	-0.0603(4)	0.43900(16)	0.0398(14)	-1.95
S2	4e	0.5000	-0.0034(5)	0.2500	0.0362(14)	-2.15
S3	8f	0.4939(3)	0.3665(4)	0.39771(18)	0.0418(14)	-2.07
S4	8f	0.7565(2)	0.3164(4)	0.32202(17)	0.0387(14)	-2.18

<sup>a</sup> U<sub>eq</sub> is defined as one-third of the trace of the orthogonalized U<sub>ij</sub> tensor.

**Table S3.** Selected band distances (Å) and band angles (°) for  $\alpha$ -Ag<sub>4</sub>P<sub>2</sub>S<sub>7</sub>.

Ag1–S1 <sup>2</sup>	2.563(3)	Ag2–S4	2.522(3)
Ag1–S3 <sup>3</sup>	2.876(3)	Ag2–S4 <sup>6</sup>	2.719(3)
Ag1–S3 <sup>4</sup>	2.593(3)	P1–S1	2.038(3)
Ag1–S4	2.538(3)	P1–S2	2.119(3)
Ag2–S1 <sup>5</sup>	2.547(3)	P1–S3	2.006(3)
Ag2–S3 <sup>2</sup>	2.699(3)	P1–S4	2.042(4)
S1 <sup>1</sup> –Ag1–S3 <sup>3</sup>	106.27(9)	S4–Ag2–S1 <sup>5</sup>	134.65(9)
S1 <sup>1</sup> –Ag1–S3 <sup>4</sup>	100.28(9)	S4–Ag2–S3 <sup>1</sup>	113.74(9)
S3 <sup>3</sup> –Ag1–S3 <sup>4</sup>	85.23(9)	S4–Ag2–S4 <sup>6</sup>	99.05(7)
S4–Ag1–S1 <sup>1</sup>	120.26(9)	S1–P1–S2	97.07(14)
S4–Ag1–S3 <sup>3</sup>	133.25(9)	S1–P1–S4	111.48(16)
S4–Ag1–S3 <sup>4</sup>	90.54(9)	S3–P1–S1	111.99(16)
S1 <sup>5</sup> –Ag2–S3 <sup>1</sup>	90.22(9)	S3–P1–S2	111.53(14)
S1 <sup>5</sup> –Ag2–S4 <sup>6</sup>	120.14(8)	S3–P1–S4	114.42(16)
S3 <sup>1</sup> –Ag2–S4 <sup>6</sup>	89.25(9)	S4–P1–S2	109.03(13)

Symmetry codes: <sup>1</sup>1/2+X,1/2+Y,+Z; <sup>2</sup>2–X,1–Y,1–Z; <sup>3</sup>1/2+X,-1/2+Y,+Z; <sup>4</sup>3/2–X,1/2–Y,1–Z;  
<sup>5</sup>+X,1+Y,+Z; <sup>6</sup>3/2–X,1/2+Y,1/2–Z

**Table S4.** Atomic coordinates, equivalent isotropic displacement parameters and bond valence sums (BVS) for  $\beta$ -Ag<sub>4</sub>P<sub>2</sub>S<sub>7</sub>.

Atom	Wyckoff position	x	y	z	U <sub>eq</sub> (Å <sup>2</sup> ) <sup>a</sup>	BVS
Ag1	6c	1.0487(2)	0.7350(2)	0.53460(4)	0.0383(4)	0.96
Ag2	6c	1.3140(2)	0.4521(2)	0.59906(5)	0.0448(4)	1.05
P1	6c	0.6260(5)	0.1252(5)	0.59747(10)	0.0136(6)	5.26
S1	6c	0.4113(6)	0.1732(6)	0.54084(11)	0.0195(6)	-1.97
S2	3a	0.3758(6)	0	0.66667	0.0153(8)	-2.12
S3	6c	0.6983(6)	-0.1294(6)	0.57003(11)	0.0241(7)	-2.10
S4	6c	0.9217(6)	0.4471(5)	0.62008(11)	0.0193(6)	-2.13

<sup>a</sup> U<sub>eq</sub> is defined as one-third of the trace of the orthogonalized U<sub>ij</sub> tensor.

**Table S5.** Selected band distances (Å) and band angles (°) for  $\beta$ -Ag<sub>4</sub>P<sub>2</sub>S<sub>7</sub>.

Ag1–S1 <sup>1</sup>	2.583(3)	Ag2–S4	2.526(3)
Ag1–S3 <sup>2</sup>	2.653(3)	Ag2–S4 <sup>5</sup>	2.812(3)
Ag1–S3 <sup>3</sup>	2.882(3)	P1–S1	2.030(4)
Ag1–S4	2.551(3)	P1–S2	2.123(3)
Ag2–S1 <sup>4</sup>	2.543(3)	P1–S3	1.996(4)
Ag2–S3 <sup>1</sup>	2.646(4)	P1–S4	2.038(4)
S1 <sup>1</sup> –Ag1–S3 <sup>2</sup>	93.89(10)	S4–Ag2–S1 <sup>4</sup>	132.65(11)
S1 <sup>1</sup> –Ag1–S3 <sup>3</sup>	104.97(10)	S4 <sup>4</sup> –Ag2–S3 <sup>1</sup>	118.13(11)
S3 <sup>3</sup> –Ag1–S3 <sup>2</sup>	86.05(9)	S4–Ag2–S4 <sup>5</sup>	93.57(7)
S4–Ag1–S1 <sup>1</sup>	121.41(9)	S1–P1–S2	96.77(17)
S4–Ag1–S3 <sup>2</sup>	88.59(10)	S1–P1–S4	111.70(18)
S4–Ag1–S3 <sup>3</sup>	133.56(11)	S3–P1–S1	110.94(16)
S1 <sup>4</sup> –Ag2–S3 <sup>1</sup>	98.04(10)	S3–P1–S2	111.92(16)
S1 <sup>4</sup> –Ag2–S4 <sup>5</sup>	118.59(10)	S3–P1–S4	115.26(18)
S3 <sup>1</sup> –Ag2–S4 <sup>5</sup>	88.08(9)	S4–P1–S2	108.74(13)

Symmetry codes: <sup>1</sup>1+X,1+Y,+Z; <sup>2</sup>+X,1+Y,+Z; <sup>3</sup>1+Y,+X,1-Z; <sup>4</sup>1+X,+Y,+Z; <sup>5</sup>1-Y+X,1-Y,4/3-Z

**Table S6.** Band gap comparison in ternary Ag-based DL chalcogenides.

Compound	Crystal system	Space group	$E_g$ (eV)	Refs.
AgGaS <sub>2</sub>	Tetragonal	$\bar{I}42d$	2.6	10
AgGaSe <sub>2</sub>	Tetragonal	$\bar{I}42d$	1.83	11
AgInS <sub>2</sub>	Tetragonal	$\bar{I}42d$	1.86	12
Ag <sub>3</sub> PS <sub>4</sub>	Orthogonal	$Pmn2_1$	2.43	13
Ag <sub>2</sub> GeS <sub>3</sub>	Orthogonal	$Cmc2_1$	2.07	14
AgFeS <sub>2</sub>	Tetragonal	$\bar{I}42d$	0.88	15
AgGaTe <sub>2</sub>	Tetragonal	$\bar{I}42d$	1.36	16
<u>AgIn<sub>5</sub>Se<sub>8</sub></u>	<u>Tetragonal</u>	- <u>P</u> <u>2m</u>	<u>1.34</u>	17
Ag <sub>4</sub> P <sub>2</sub> S <sub>7</sub>	Trigonal	$P3_221$	2.9	This work

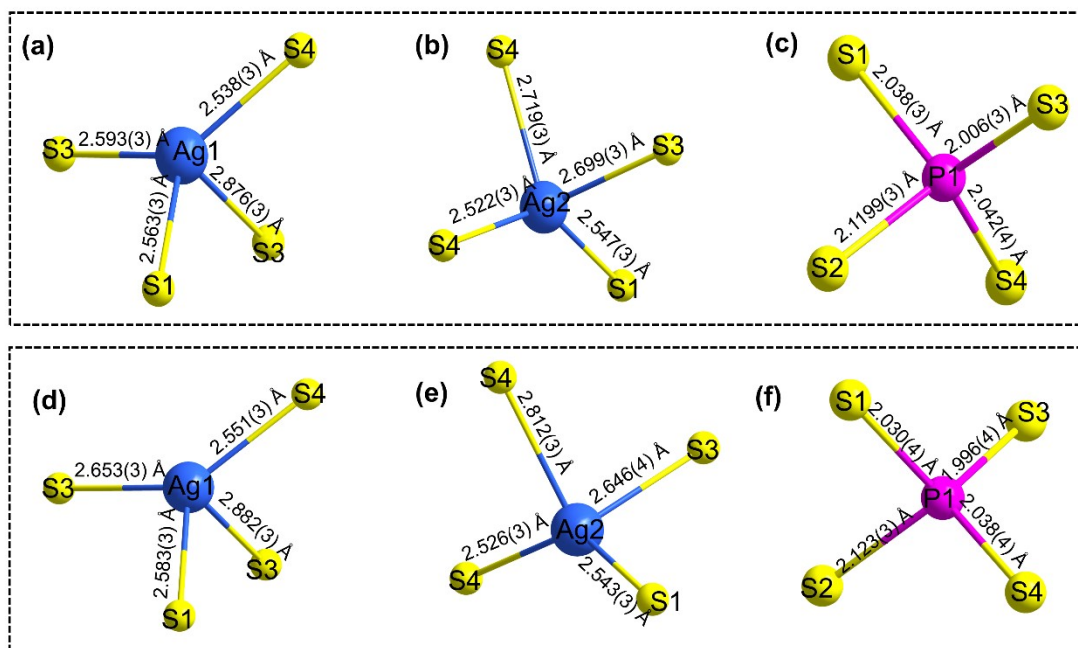


**Fig. S1** The coordination environments of Ag1, Ag2, and P atoms of  $\alpha$ - $\text{Ag}_4\text{P}_2\text{S}_7$  (a, b, and c) and  $\beta$ - $\text{Ag}_4\text{P}_2\text{S}_7$  (d, e, and f).

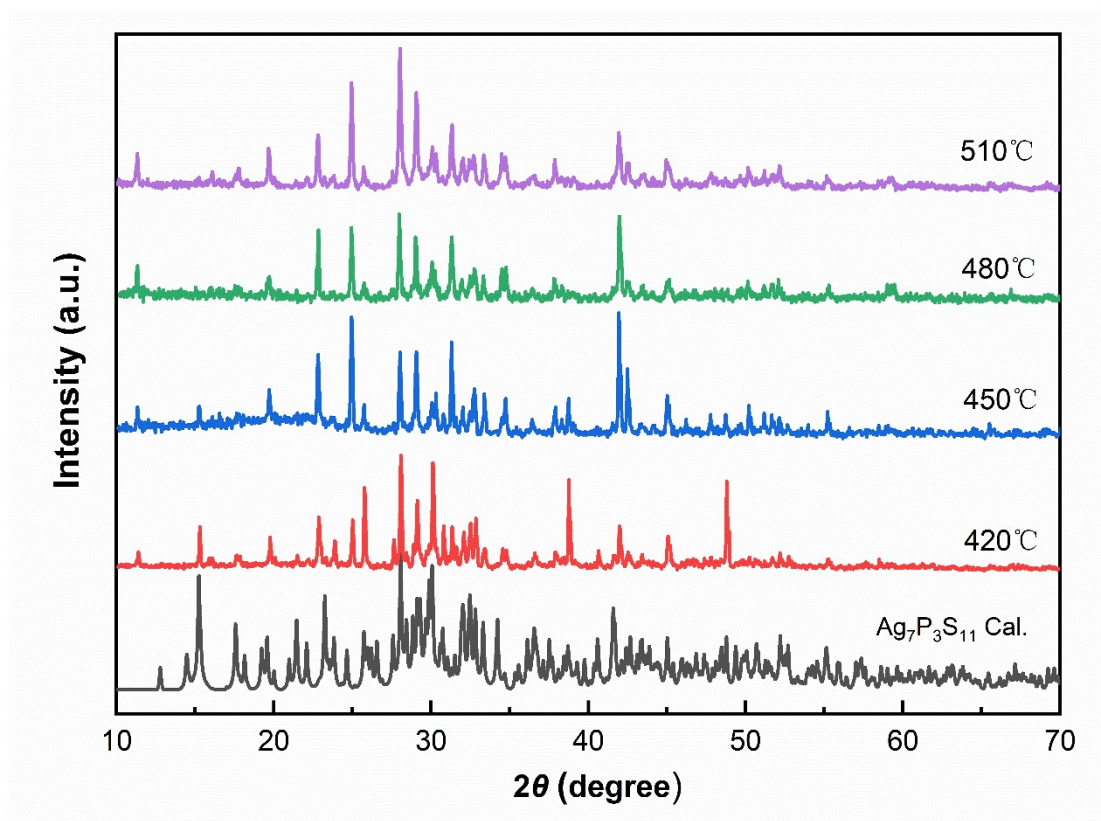


**Fig. S2** Peritectic reaction of  $\text{Ag}_7\text{P}_3\text{S}_{11}$  and melt.

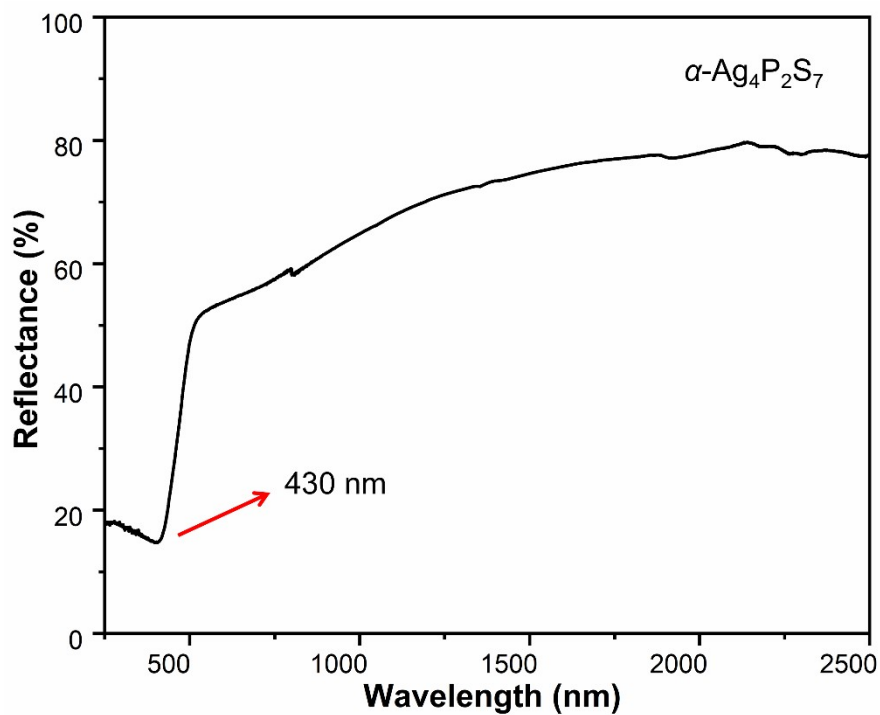


Fig. S3 UV-vis-NIR diffuse reflectance spectra-spectrum of  $\alpha\text{-Ag}_4\text{P}_2\text{S}_7$ .

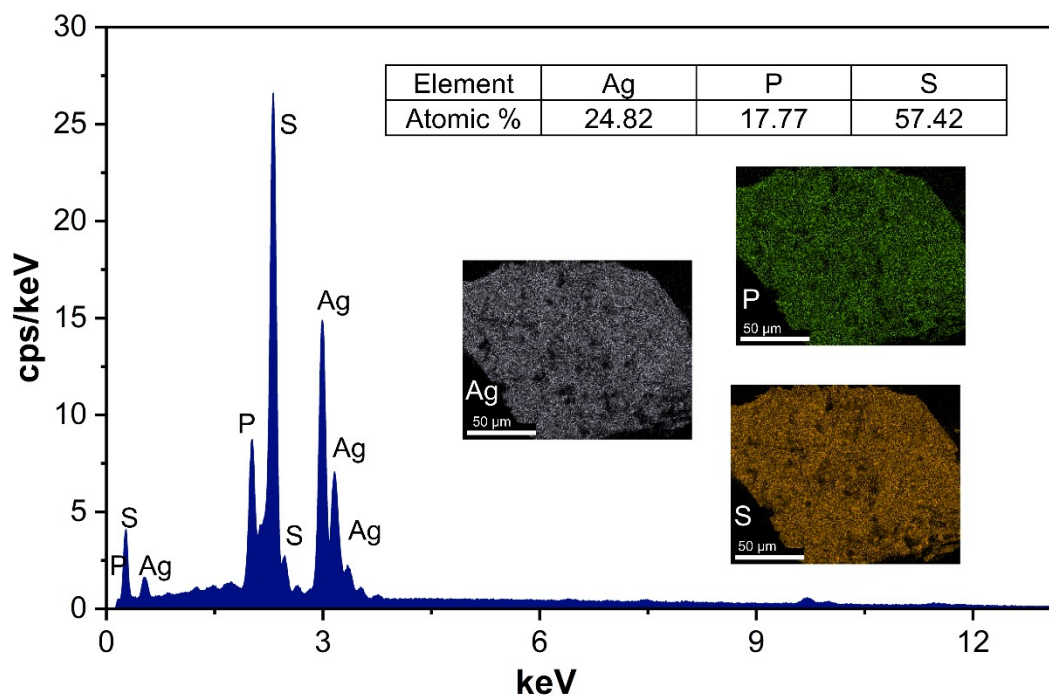
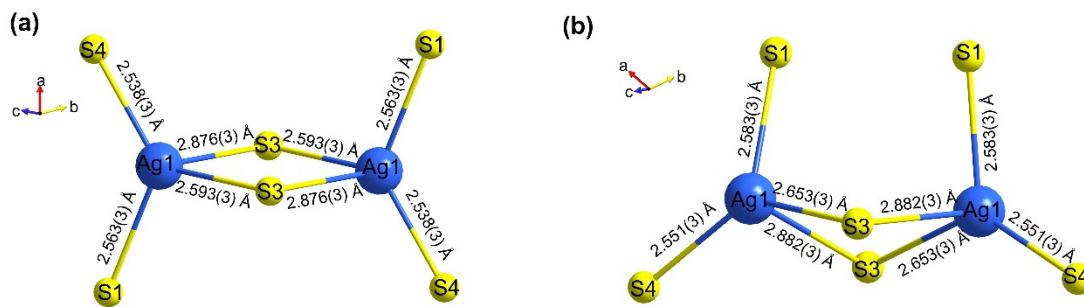
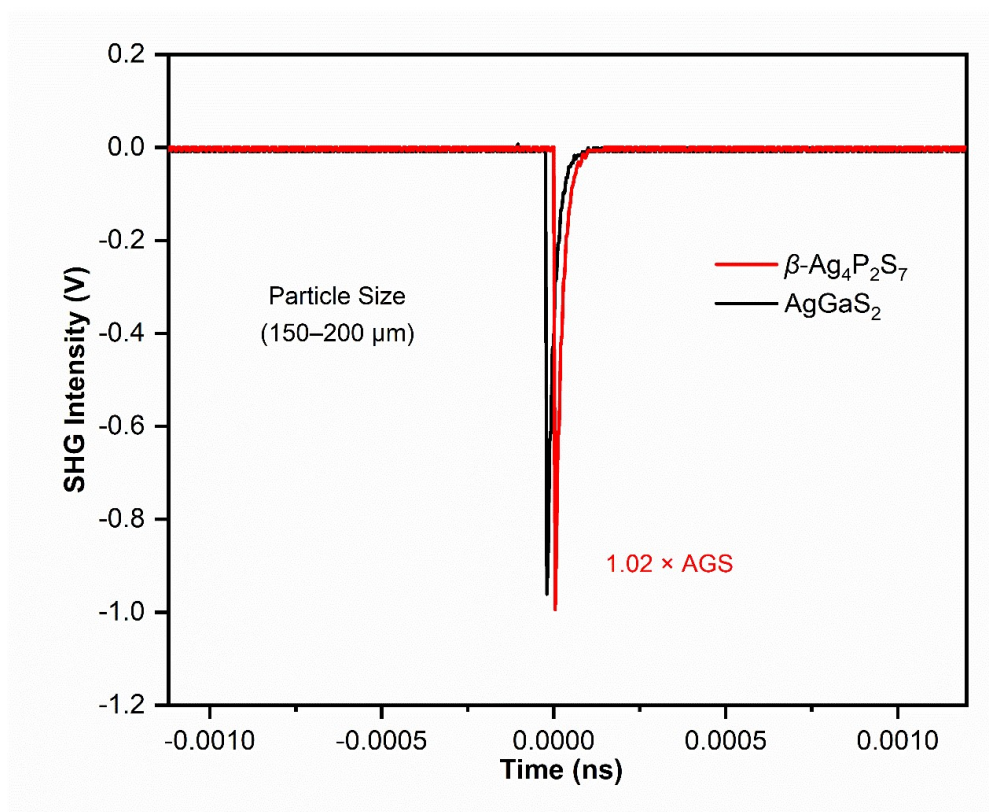


Fig. S4 The SEM pictures and EDS results of  $\beta\text{-Ag}_4\text{P}_2\text{S}_7$ .



**Fig. S5** The coordination environments of  $[Ag_1S_4]^{7-}$  bridges in (a)  $\alpha$ - $Ag_4P_2S_7$  and (b)  $\beta$ - $Ag_4P_2S_7$ .



**Fig. S6** SHG signals to compare between  $\beta$ - $Ag_4P_2S_7$  and references at the particle size of 150–200  $\mu$ m.

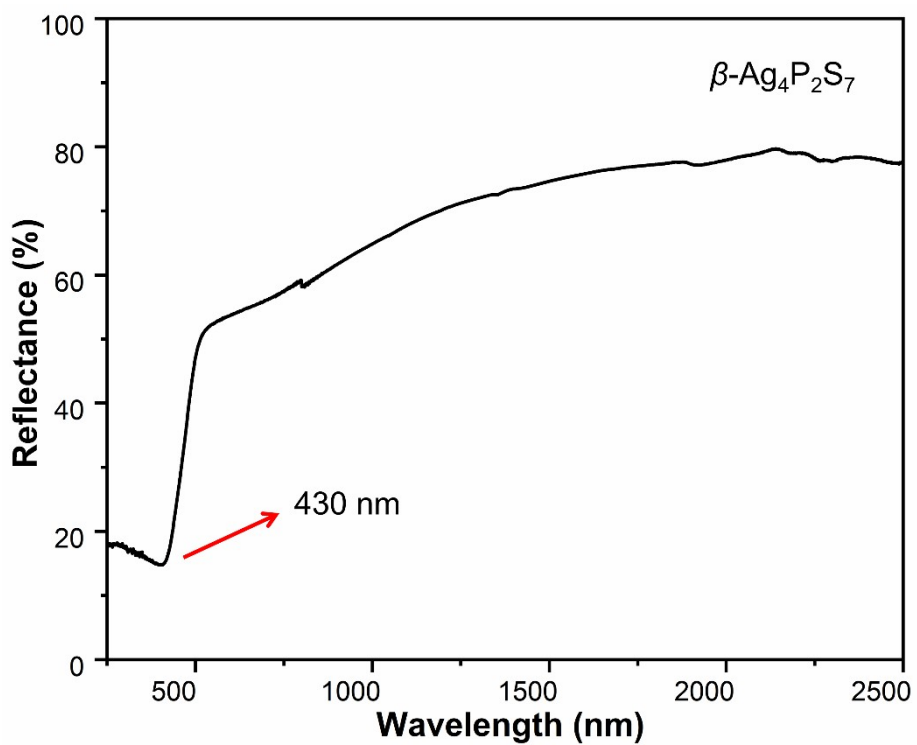


Fig. S7 UV-vis-NIR diffuse reflectance spectra-spectrum of  $\beta\text{-Ag}_4\text{P}_2\text{S}_7$ .

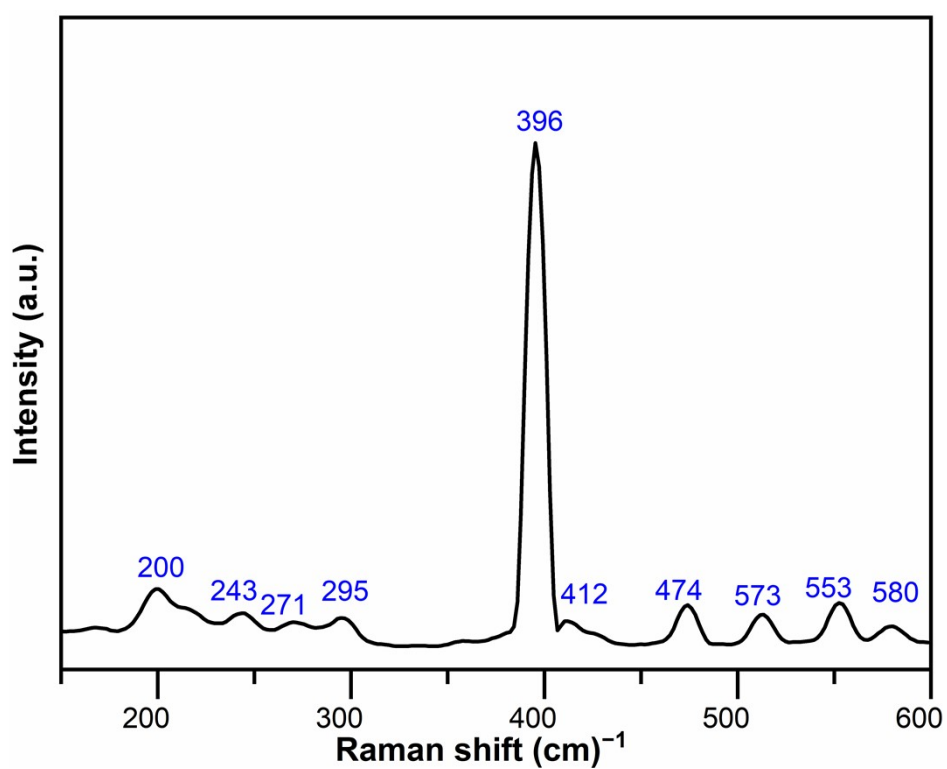


Fig. S8 Raman spectrum of  $\beta\text{-Ag}_4\text{P}_2\text{S}_7$ .

## Reference

1. E. L. Simmons, Diffuse reflectance spectroscopy: a comparison of the theories, *Appl. Opt.*, 1975, **14**, 1380-1386.
2. S. K. Kurtz and T. T. Perry, A powder technique for the evaluation of nonlinear optical materials, *J. Appl. Phys.*, 1968, **39**, 3798-3813.
3. S. J. Clark, M. D. Segall, C. J. Pickard, P. J. Hasnip, M. J. Probert, K. Refson and M. C. Payne, First principles methods using CASTEP, *Zh. Fiz. Khim.*, 2005, **220**, 567-570.
4. W. Kohn and L. J. Sham, Self-consistent equations including exchange and correlation effects, *Phys. Rev.*, 1965, **140**, A1133-A1138.
5. J. P. Perdew, K. Burke and M. Ernzerhof, Generalized gradient approximation made simple, *Phys. Rev. Lett.*, 1996, **77**, 3865-3868.
6. P. E. Blochl, Projector augmented-wave method, *Phys. Rev. B.*, 1994, **50**, 17953-17979.
7. D. Hamann, M. Schlüter and C. Chiang, Norm-conserving pseudopotentials, *Phys. Rev. Lett.*, 1979, **43**, 1494-1497.
8. R. W. Godby, M. Schlüter and L. Sham, Self-energy operators and exchange-correlation potentials in semiconductors, *Phys. Rev. B.*, 1988, **37**, 10159.
9. R. He, Z. S. Lin, M. H. Lee and C. T. Chen, Ab initio studies on the mechanism for linear and nonlinear optical effects in  $\text{YAl}_3(\text{BO}_3)_4$ , *J. Appl. Phys.*, 2011, **109**, P103510.
10. H. M. Zhou, L. Xiong, L. Chen and L. M. Wu, Dislocations that decrease size mismatch within the lattice leading to ultrawide band gap, large second-order susceptibility, and high nonlinear optical performance of  $\text{AgGaS}_2$ , *Angew. Chem. Int. Ed.*, 2019, **58**, 9979-9983.
11. G. C. Catella, L. R. Shiozawa, J. R. Hietanen, R. C. Eckardt, R. K. Route, R. S. Feigelson, D. G. Cooper and C. L. Marquardt, Mid-IR absorption in  $\text{AgGaSe}_2$  optical parametric oscillator crystals, *Appl. Opt.*, 1993, **32**, 3948-3951.
12. J. Shay, B. Tell, L. Schiavone, H. Kasper and F. Thiel, Energy bands of  $\text{AgInS}_2$  in the chalcopyrite and orthorhombic structures, *Phys. Rev. B.*, 1974, **9**, 1719.
13. Y. Yang, B. B. Zhang, X. W. Wu and K. Wu, A series of  $\text{M}_3\text{PS}_4$  ( $\text{M} = \text{Ag}, \text{Cu}$  and  $\text{Ag/Cu}$ ) thiophosphates with diamond-like structures exhibiting large second harmonic

- generation responses and moderate ion conductivities, *Dalton Trans.*, 2021, **50**, 4129-4132.
14. H. Chen, M. Y. Ran, S. H. Zhou, X. T. Wu and H. Lin, Ag<sub>2</sub>GeS<sub>3</sub>: a diamond-like chalcogenide as an IR nonlinear optical material with outstanding second-harmonic generation response, *Adv. Opt. Mater.*, 2024, **12**, 2401100.
  15. S. Beniamino, Transformation of Ag nanowires into semiconducting AgFeS<sub>2</sub> nanowires, *J. Am. Chem. Soc.*, 2015, **137**, 4340-4343.
  16. B. Tell, J. L. Shay and H. M. Kasper, Some properties of AgAlTe<sub>2</sub>, AgGaTe<sub>2</sub>, and AgInTe<sub>2</sub>, *Phys. Rev. B.*, 1974, **9**, 5203-5208.
  17. L. F. Dong, S. Z. Zhang, P. F. Gong, F. Liang and Z. S. Lin, AgIn<sub>5</sub>Se<sub>8</sub>: a defect diamond-like non-linear optical selenide, *Inorg. Chem. Front.*, 2023, **10**, 3248-3254.